Acta Astronautica 119 (2016) 241–251

Contents lists available at ScienceDirect

Acta Astronautica

journal homepage: www.elsevier.com/locate/actaastro

Determination of the force transmitted by an ion thruster plasma plume to an orbital object

A. Alpatov [a], F. Cichocki [b], A. Fokov [a], S. Khoroshylov [a], M. Merino [b,*], A. Zakrzhevskii [c]

[a] Institute of Technical Mechanics NAS of Ukraine & SSA of Ukraine, Dnipropetrovsk, Ukraine
[b] Equipo de Propulsión Espacial y Plasmas, Universidad Carlos III de Madrid, Leganés, Spain
[c] S. P.Timoshenko Institute of Mechanics NAS of Ukraine, Kiev, Ukraine

ARTICLE INFO

Article history:
Received 21 March 2015
Received in revised form
11 November 2015
Accepted 17 November 2015
Available online 27 November 2015

Keywords:
Electric propulsion
Plasma plume
Contactless
Space debris
Active debris removal
Ion beam shepherd

ABSTRACT

An approach to determine the force transmitted by the plasma plume of an ion thruster to an orbital object immersed in it using its central projection on a selected plane is proposed. A photo camera is used to obtain the image of the object central projection. The algorithms for the calculation of the transmission of momentum by the impacting ion beam are developed including the determination of the object contour and the correction of the error due to a camera offset from the ion beam axis, and the computation of the fraction of the ion beam that impinges on the object surface.

1. Introduction

As a result of space activity, near-Earth space is littered by a considerable quantity of artificial objects and their fragments, which do not execute any useful function (fragments of upper stages of launch vehicles, non-functioning spacecraft, etc.). Recent research on the modelling of the population of space debris (SD) shows that the situation for some Earth orbits is critical already. For example, results of the official research conducted by the Inter-Agency Space Debris Coordination Committee in 2012 show that the number of SD objects in low Earth orbits that will form in the future as a result of collisions will exceed the number of objects that decay and reenter into the atmosphere as a result of natural processes [1]. This fact indicates that the mitigation measures approved by the majority of space nations for future missions are insufficient to avoid the continued growth of SD. In view of this, the space community is seriously considering different strategies for active SD removal.

A number of proposed concepts of active removal of orbital fragments are described in the literature, from laser systems [2,3] to electrodynamic tethers [4–8]. While docking or grabbing the target object by means of auxiliary devices (for example, a net or a harpoon) is the most obvious means of deorbiting them, this operation may be technologically difficult and unsafe because SD objects are uncontrollable, may have a complex rotational motion around the centre of mass, and differ substantially in shape and mechanical properties.

In order to avoid the described complexity, a concept of contactless removal of SD objects named “ion beam shepherd” (IBS) [9] has been proposed. The principle of this concept consists in using a high-velocity jet of ions from a gridded ion thruster (GIT) as a means for transmitting momentum to the object to be removed (the

* Corresponding author. Tel.: +34 91624 8237.
E-mail address: mario.merino@uc3m.es (M. Merino).

http://dx.doi.org/10.1016/j.actaastro.2015.11.020
0094-5765/

target), in order to reposition it or force its reentry in the atmosphere. The IBS concept has a number of advantages in comparison with other concepts, namely: acceptable deorbiting performance [9], a low risk level, reusability (multimission) capabilities, and technological readiness.

One of the key problems arising in the research of the IBS concept is the modelling and determination of the force transmitted by the shepherd to the SD. Accurate information on this force is necessary both for the successful realisation of the chosen removal programme and for the navigation and control of the relative motion of the "shepherd – SD object" system.

Since this problem is relatively new, the literature devoted to it is still small. For example, an instrument for the direct experimental determination of the momentum transferred to a target by energetic atoms or ions is presented in [10]. In [11–13] the theoretical foundations of a GIT plume and calculations of the transmitted force are proposed. In [14] analytical expressions of the force on a spherical SD object are obtained. Authors of these publications integrate directly the transmitted forces on the object surface, which is known a priori. However, application of these force determination techniques on board the shepherd is inconvenient for two reasons: firstly, the necessary information about the exact shape, size, and orientation of the object may not be fully available before the mission starts. Secondly, the computational power needed to run these calculations in real-time sets a strong requirement on the system.

This paper presents a simple alternative approach to determine the transmitted force from far less information about the target object, namely its central projection on an auxiliary plane perpendicular to the ion beam axis. This approach allows simplifying the force computation and can be implemented on board the shepherd with the help of a visual camera. The objective of the present work is to develop the algorithm for the calculation of the force and characterize its features for IBS contactless removal of SD.

The remainder of this paper is organised as follows. Section 2 describes the mechanism of the interaction of the ion beam with the target. The model of plasma plume expansion is presented in Section 3. The new approach to determine the force transmitted by the plasma plume to a target using its central projection is described in Sections 4 and 5. Section 6 validates the proposed approach numerically. The problem of the determination of the target contour from a photo is addressed in Section 7. The algorithm for the calculation of the transmitted force is summarised in Section 8. Finally, conclusions are gathered in Section 9.

2. Interaction of the ion beam with the target object

The ion beam of a GIT consists of a quasineutral jet of propellant ions (typically xenon), accelerated to energy levels of a few keV, and neutralising electrons. A rigid body immersed in this plasma jet receives a net force, which can be used to change its state of motion contactlessly.

When ions reach the target surface, several phenomena can take place. Firstly, most ions penetrate into the material of the SD and subsequently stop within a distance of several nanometres from its surface. In doing so, they deliver their momentum and energy to the SD. After an accommodation time, the neutralised ions leave the material and escape the target surface at thermal speeds. Secondly, depending on their energy and angle, impacting ions can also sputter the surface of the SD, releasing some of its atoms into space. The velocity of the sputtered materials range between the thermal velocity of the surface and the impacting ion velocity. Thirdly, a small fraction of the incoming ions can bounce back at the surface if their angle and conditions are right. Lastly, the electron population of the plasma jet exerts a pressure force on the SD.

Of all these phenomena that can create a force on the target, the momentum of the incoming ions is the dominant one: escaping neutralized ions and sputtered materials have a much lower velocity; backscattered ions make up only a small fraction of the population; and electron pressure has a negligible effect in a hypersonic plasma jet (where ion inertia is much larger than electron pressure). These secondary contributions are small and act as to increase the total force transmitted to the object, so they can be conservatively neglected in a first approach. Hence, in the following only the force caused by the incoming ion momentum will be kept. The other contributions could still be taken into account phenomenologically as an empirical multiplier factor on the incoming ion momentum.

Under these simplifying assumptions, the elementary force transmitted to a differential area of SD object may be calculated as follows [14]:

$$\mathbf{dF} = mn\mathbf{U}(-\mathbf{V}\cdot\mathbf{U})ds, \tag{1}$$

where m is the ion mass; n is the ion number density; $\mathbf{U}$ is the ion velocity vector; ds is the elementary area of surface of the target; $\mathbf{V}$ is the unit normal vector to the elementary area.

The force $\mathbf{F}$ transmitted to the target by the ion beam can be calculated as the integral of elementary forces (1) on the irradiated surface of the target S:

$$\mathbf{F} = \int_S \mathbf{dF}. \tag{2}$$

3. Ion beam model

The plasma plume can be roughly divided into the near region (usually less than 0.5 m from the GIT) and far region (downstream of it) [11,12]. Modelling the near region requires to consider the influence of the GIT electromagnetic fields, the neutraliser, and the local non-uniformity of plasma. Within this region, a smooth, single-peaked plasma density profile gradually forms and the jet adquires its initial divergence angle. In the far region the influence of these effects becomes insignificant; the distribution of plasma and the slow increase of beam divergence angle depend essentially on its residual electron pressure and the ambipolar electric field. The beam

far region is the region of interest for the problem of contactless removal of the SD considered in this paper, since the plasma-target interaction occurs there.

There are several mathematical models with different degrees of complexity and accuracy [13] for the description of the far region of the ion beam. The so-called self-similar model for the plasma distribution can be chosen as a compromise for the purposes of this study. Self-similar models are based on the assumption that the plasma expansion can be described through a dimensionless self-similarity function $h(\tilde{z})$, so that ion streamlines (r, z) can be expressed as follows:

$$r(z) = r_0 h(\tilde{z}),\ \tilde{z} = z/R_0,$$

where r_0 is the initial radius of the streamline at a chosen reference normal plane in the far region (where we take $z = 0$), and R_0 is the radius at that plane of the plasma tube that contains 95% of the ion beam mass flow. Note that $h(0) = 1$ so that $r(0) = r_0$.

In a hypersonic plasma beam, i.e. in the limit where the ion Mach number is very large, the axial ion acceleration is small, and as a first approximation the axial component of the ion velocity can be assumed constant and equal to its value at the origin:

$$u_z = u_{z0} = \text{const}. \tag{3}$$

Using the $h(\tilde{z})$ function, a possible solution for the radial component of the velocity and the plasma density is [13]:

$$u_r = u_z \tilde{r} \frac{h'}{h}, \tag{4}$$

$$n = \frac{n_0}{h^2(\tilde{z})} \exp\left(-C \frac{\tilde{r}^2}{2h^2(\tilde{z})} \right), \tag{5}$$

where $\tilde{r} = r/R_0$; n_0 is the plasma density at $z = r = 0$, and $C \cong 6$ is an integration constant. Under the assumption that the electron temperature T_e remains constant in the far region, the self-similarity function $h(\tilde{z})$ is the solution of the following differential equation:

$$h' = \sqrt{\tan^2 \alpha_0 + \frac{2C}{M_0^2} \ln h}, \tag{6}$$

where h' is the derivative of the function $h(\tilde{z})$ with respect to $\tilde{z}$; α_0 is the initial divergence angle of the 95% beam streamtube (defined as the angle of that tube with respect to the axis); and $M_0 = u_0/\sqrt{T_e/m}$, u_0 are the ion Mach number and the ion velocity at the origin.

It is highlighted that h' increases as $1/M_0^2$ downstream, and therefore the ion beam approaches a cone when $M_0 \gg 1$ (hypersonic plasma). For typical GIT values ($M_0 \geq 30$) and distances to the target less than 7 m, it is safe to assume that the beam is conical with very little error. In this case the self-similarity function can be approximated as:

$$h = 1 + \tilde{z} \tan \alpha_0, \tag{7}$$

and the effective beam vertex is located at $\tilde{z} = -1/\tan \alpha_0$.

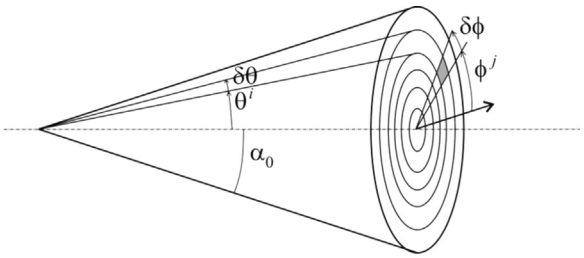

Fig. 1. Partition of ion beam into finite elements.

4. Central projection of the target

As noted above, when $M_0 \gg 1$ the shape of the ion beam can be approximated by a cone. Moreover, in the limit $M_0 \to \infty$ both components of the ion velocity remain constant on each streamline, so ions do not change their momentum in the expansion. Because the plasma properties depend on the angle from the axis of the beam, we will divide the cone into finite elements in spherical coordinates, as shown in Fig. 1.

Here θ^i is the discrete polar angle, $\delta\theta$ is the step of the polar discretisation, ϕ^j is the discrete azimuthal angle, $\delta\phi$ is the step of the azimuthal discretisation. The contribution to the transmitted force of the last 5% of the plasma mass flow is insignificant for the task under consideration and is conservatively neglected.

It is clear that the cone cross-section increases with the square of the distance from the vertex of the cone. After substituting the expression for the self-similarity function (7) in (5) one can see that the plasma density decreases in inverse proportion to the square of the distance $(\tilde{z} + 1/\tan \alpha_0)$ from the vertex of the cone. Considering the described mechanism of interaction of the beam with the target surface, and also taking into account the two previous statements, we can assert that the elementary force acting on the elementary surface ds of the target is equal to the elementary force acting on a central projection of this surface on any plane perpendicular to the axis of the beam.

Hence, for the calculation of the force it is possible to use just a central projection on a perpendicular plane, instead of the full 3D target surface. This simplification is central to the approach for force calculation derived in this paper.

It is obvious that if all rays emanating from the plume vertex hit the target, the force that acts on it is directed along the axis of the beam and is equal to the full GIT thrust. If only the ions from some elemental ray $\delta\theta \times \delta\phi$ hit in the target, the direction of the resulting force coincides with the ray. In this spirit, to approximate the force over the SD it is enough to sum all forces created by the elementary components of the beam that intersect the central projection of the target on a projection plane (Fig. 2).

To continue with the derivation of the force model, we will introduce the following right-handed orthogonal frames of reference:

The frame $O_P x_P y_P z_P$ is fixed to the chosen plane of projection (F_P), O_P is the intersection of the plane and the axis of the beam. The axis $O_P z_P$ is perpendicular to the

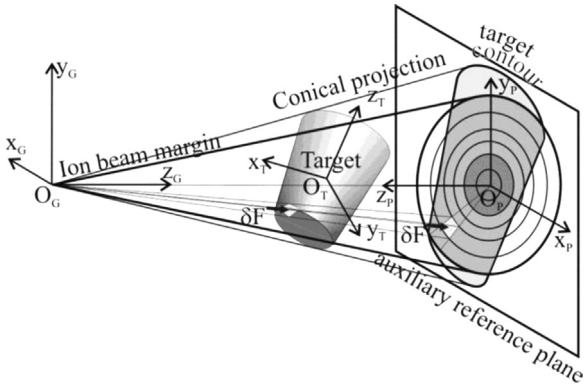

Fig. 2. Central projection of target on auxiliary plane.

plane of projection and is directed toward the target, axes O_Px_P and O_Py_P lie in the projection plane.

The frame $O_Gx_Cy_Gz_G$ whose origin O_G is in vertex of the imaginary cone of the beam is fixed to the GIT (F_G). The axis O_Gz_G coincides with the axis of the beam and is directed toward the target. Axes O_Px_P and O_Gx_G, O_Py_P and O_Gy_G are parallel.

$O_Tx_Ty_Tz_T$ is an arbitrary frame that is fixed on the target (F_T). The attitude of F_T axes with respect to F_G is defined by Euler angles φ, ϑ, ψ. The matrix corresponding to these rotations is

$$T_{TG} = T_\psi T_\varphi T_\vartheta,$$

where

$$T_\psi = \begin{bmatrix} \cos\psi & \sin\psi & 0 \\ -\sin\psi & \cos\psi & 0 \\ 0 & 0 & 1 \end{bmatrix};$$

$$T_\phi = \begin{bmatrix} 1 & 0 & 0 \\ 0 & \cos\varphi & \sin\varphi \\ 0 & -\sin\varphi & \cos\varphi \end{bmatrix}; \; T_\vartheta = \begin{bmatrix} \cos\vartheta & 0 & -\sin\vartheta \\ 0 & 1 & 0 \\ \sin\vartheta & 0 & \cos\vartheta \end{bmatrix}.$$

Let us approximate the target surface by a mesh of finite surface elements. The mesh here is understood as the topological set of L points, connected by edges, segments of straight lines, so that the initial surface is divided into elements of a defined shape. The choice of the partition method depends on the complexity of the target. For example, in case of a cylindrical shape it is enough to set certain amount of points to define the bases of the cylinder. For targets of arbitrary shapes, triangulation methods [15] can be used instead.

The position vectors defining a set of points of the target in F_G can be found as follows:

$$\mathbf{P}^l_G = \mathbf{T}_{TG}\mathbf{P}^l_T + \mathbf{B}_{TG}, \; l = 1, \ldots, L;$$

where $\mathbf{P}^l_T$ are the vectors defining a set of target points in F_T; $\mathbf{B}_{TG}$ is the vector defining position of F_T origin in F_G; l runs over all points.

The coordinates P^l_G of the target points, which are projected on the considered plane, are defined as follows:

$$x^l_P = f\frac{x^l_G}{z^l_G}, \; y^l_P = f\frac{y^l_G}{z^l_G}, \tag{8}$$

where f is the distance between the origins of F_P and F_G; x^l_G, y^l_G, z^l_G are the coordinates of the points of the target in F_G; x^l_P, y^l_P are the coordinates of the central projections of the points of the target on this plane in F_P.

5. Evaluation of the transmitted force on the central projection of the target

The boundaries of the ring elements of the central projection of a beam (Fig. 1) can be described with the use of the parametrical equation of a circle. The radius of the i-th ring element is defined as follows

$$R^i = f \tan\theta^i, \; 0 \le \theta^i \le \alpha_0, \; i = 1, \ldots, I,$$

where I is the number of ring elements.

The divergence angle of the i-th conic element of the beam can be expressed as follows:

$$\theta^i = i\delta\theta.$$

The set of points that approximate the projection of the mesh of finite elements will be described as:

$$\begin{cases} x^{ij}_P = R^i \cos\phi^j \\ y^{ij}_P = R^i \sin\phi^j \end{cases}, \; j = 1, \ldots, J, \; 0 \le \phi^j < 2\pi. \tag{9}$$

The discrete angle of the parametrical equation of the circle (9) is defined as follows:

$$\phi^j = j\delta\phi, \; j = 0, \ldots, J-1,$$

where J is number of sectors in the beam.

As seen in Fig. 1, the finite elements defined by three points with coordinates (x^0_P, y^0_P), $\left(x^{1,j}_P, y^{1,j}_P\right)$ and $\left(x^{1,j+1}_P, y^{1,j+1}_P\right)$ represent sectors of circles with radius R^1, and the elements characterised by four points with coordinates $\left(x^{i,j}_P, y^{i,j}_P\right)$, $\left(x^{i,j}_P, y^{i,j}_P\right)$, $\left(x^{i+1,j}_P, y^{i+1,j}_P\right)$ and $\left(x^{i+1,j+1}_P, y^{i+1,j+1}_P\right)$ are truncated sectors. Hence, the area of these elements can be calculated accordingly:

$$ds^{1,i} = \left(R^1\right)^2 \delta\theta \text{ and } ds^{i+1j} = \left(\left(R^{i+1}\right)^2 - \left(R^i\right)^2\right)\delta\theta, \; i = 1, \ldots, I-1,$$

$$j = 0, \ldots, J-1. \tag{10}$$

As mentioned above, the beam can hit the target only partially. In that case, not all the elementary components of the projection of the beam will fall within the contour of the target projection and, hence, it is necessary to identify these elements. For this purpose, from the set of all points P^l_P of the target that are projected on the considered plane, we will first select the K points C^l_P ($k = 1, \ldots, K$) that define a polygon that best approximates the contour of the target projection.

When the target is a convex body, the contour of its projection can be found by determining its convex hull, a fundamental problem in computational geometry for which efficient algorithms are well developed [16].

For a target of arbitrary shape there are simple and effective algorithms for the construction of nonconvex envelopes to characterize its projection on a plane [17]. The Delaunay triangulation [16] lies at the basis of these

algorithms. The shape produced by these algorithms is controlled by a single normalised parameter, which can be used to generate a family of shapes, varying between its convex hull at one extreme and a shape with minimum area. The efficiency of these algorithms is comparable with optimum algorithms for the construction of the convex hulls, namely, the number of evaluations is proportional to $O(N \log N)$, where N is the number of input points. Nevertheless, it is necessary to notice that the assumption of convexity allows to use a smaller number of points to approximate its surface, and, hence, to reduce significantly the calculation time.

In order to identify the beam projection elements bounded by the target contour it is possible to use known algorithms from computational geometry for the point-in-polygon problem [18]. We will consider that an element of the beam is inside the area bounded by the contour if three points of a sector element with the coordinates (x_P^0, y_P^0), $\left(x_P^{1,j}, y_P^{1,j}\right)$, $\left(x_P^{1,j+1}, y_P^{1,j+1}\right)$ or four points of a truncated sector element with the coordinates $\left(x_P^{i,j}, y_P^{i,j}\right)$, $\left(x_P^{i,j+1}, y_P^{i,j+1}\right)$, $\left(x_P^{i+1,j}, y_P^{i+1,j}\right)$, $\left(x_P^{i+1,j+1}, y_P^{i+1,j+1}\right)$ lie inside the polygon with vertices C_P^k.

With the use of expressions (3) and (4) the velocity vector of ions acting on an elementary area of a target, in F_G, is defined as

$$\mathbf{U}_G^{ij} = \left[u_0 \frac{\hat{x}_G^{i,j}}{f};\ u_0 \frac{\hat{y}_G^{i,j}}{f};\ u_0\right]^T, \tag{11}$$

where $\hat{x}_G^{i,j}$, $\hat{y}_G^{i,j}$ are the coordinates of the centre of the elementary area in F_G, which are calculated as follows

$$\hat{x}_T^{i,j} = \frac{2x_P^0 + x_P^{i,j} + x_P^{i,j+1}}{4},\ \hat{y}_T^{i,j} = \frac{2y_P^0 + y_P^{i,j} + y_P^{i,j+1}}{4},\ \forall\, i = 1,$$
$$\hat{x}_T^{i,j} = \frac{x_P^{i-1,j} + x_P^{i-1,j+1} + x_P^{i,j} + x_P^{i,j+1}}{4},$$
$$\hat{y}_T^{ij} = \frac{y_P^{i-1,j} + y_P^{i-1,j+1} + y_P^{i,j} + y_P^{i,j+1}}{4},\ \forall\, i > 1.$$

Table 1
Values of the coordinates of the geometric centre and the attitude parameters of the target.

Case no.	Coordinates of geometric centre			Attitude parameters		
	b_T^x, м	b_T^y, м	b_T^z, м	ϑ, deg	φ, deg	ψ, deg
1	0	0	7	0	0	0
2	0	0.5	7	0	0	0
3	0	1	7	0	0	0
4	0	0	7	45	0	0
5	0	0.5	7	45	0	0
6	0	1	7	45	0	0
7	0	0	7	45	45	0
8	0	0.5	7	45	45	0
9	0	1	7	45	45	0
10	0	0	7	45	45	45
11	0	0.5	7	45	45	45
12	0	1	7	45	45	45
13	0	0	7	90	45	45
14	0	0.5	7	90	45	45
15	0	1	7	90	45	45

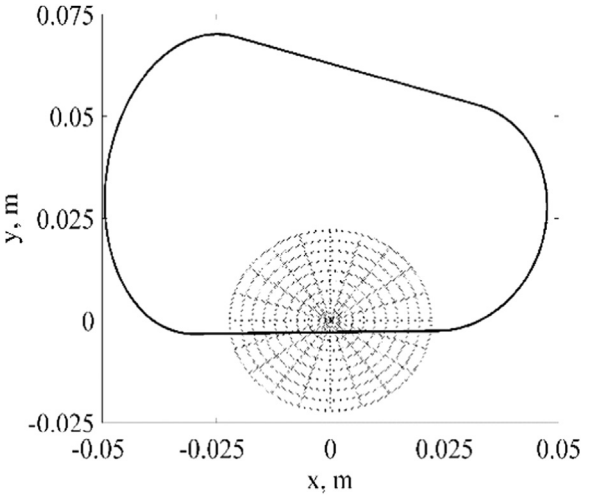

Fig. 4. Case no. 6.

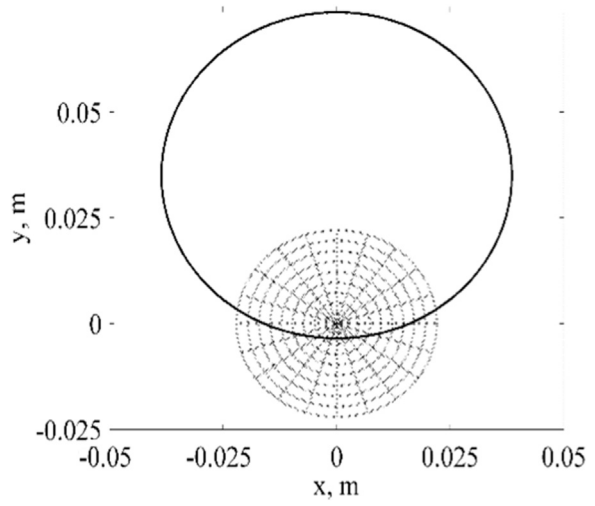

Fig. 3. Case no. 3.

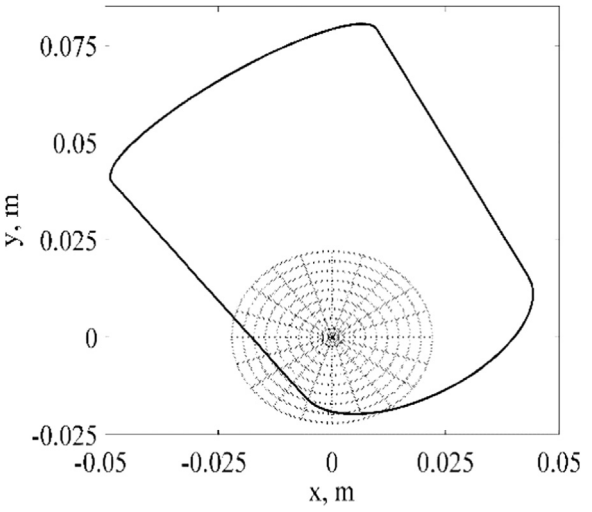

Fig. 5. Case no. 9.

After discretizing, the force acting on an elementary area may be defined according to the differential expressions:

$$\mathbf{dF}_G^{i,j} = mn^{i,j}\mathbf{U}_G^{i,j}\left(-\mathbf{V}_G^0 \cdot \mathbf{U}_G^{i,j}\right)ds^{i,j}, \tag{12}$$

$$n^{i,j} = \frac{n_0 R_0^2}{f^2 \tan^2\alpha_0}\exp\left(-C\frac{\left(\hat{x}_G^{i,j}\right)^2 + \left(\hat{y}_G^{i,j}\right)^2}{2f^2\tan^2\alpha_0}\right), \tag{13}$$

where $\mathbf{V}_G^0 = [0;\ 0;\ -1]^T$ is the unit vector of the normal to the plane, which is perpendicular to the ray.

Finally, the force acting on the target is calculated as:

$$\mathbf{F}_G = \sum_{i=1}^{I}\sum_{j=0}^{J-1}\mathbf{dF}_G^{i,j}. \tag{14}$$

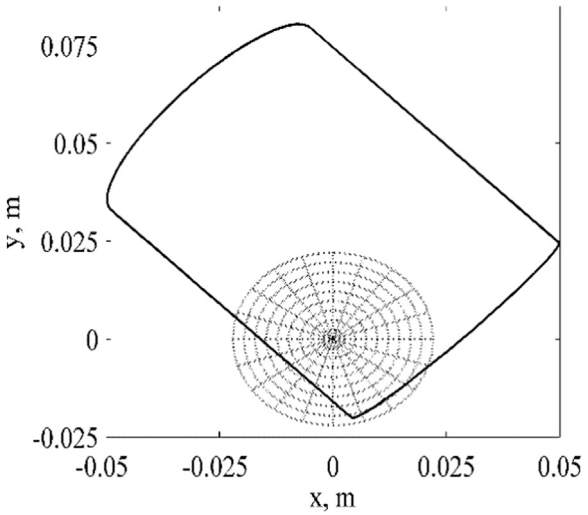

Fig. 6. Case no. 15.

6. Validation results

To validate the approach presented above the transmitted force is calculated using two methods. Method no. 1 is based on the direct integration of the force over the target surface. Method no. 2 uses the central projection of the target. A target of cylindrical shape and the following input data are used for carrying out of the calculations.

The height of the cylinder is $h=2.6$ m. The diameter of the base of the cylinder is $d=2.2$ m. The distance between the centre of projection and the projection plane is $f=0.2$ m.

The parameters of the GIT are the following: the initial 95% plasma beam radius $R_0 = 0.0805$ m; the ion mass (Xenon) $m = 2.18\cdot 10^{-25}$ kg; the initial plasma density $n_0 = 4.13\cdot 10^{15}$ m^{-3}; the initial axial velocity of ions $u_0 = 71580$ m/s; the ion Mach number is assumed large enough so that the hypersonic conic approximation for the beam can be used; the initial divergence angle of the beam is $\alpha_0 = 7^\circ$.

Values of the Euler angles and the components b_T^x, b_T^y, b_T^z of the vector B_T^{MT} for different cases which are used for the validation are presented in Table 1. The central projection of the target and the beam for some from these cases are depicted in Figs. 3–6.

Absolute and relative calculation errors are used to compare the results. The components of the absolute error vector are defined as follows

$$\Delta f^k = f_1^k - f_2^k,\ k = x, y, z,$$

where the subscript indicates the number of the method. The relative error is written in the form:

$$\delta f^k = \left|\Delta f^k / f_1^k\right|\cdot 100\%.$$

The values of the transmitted force calculated using both Method nos. 1 and 2 are presented in Table 2. The surface of the cylinder was divided into 68,802 elementary areas to apply Method no. 1. The ion beam projection was

Table 2
Transmitted forces calculated using Method nos. 1 and 2.

No.	Method no. 1			Method no. 2		
	f^x, N	f^y, N	f^z, N	f^x, N	f^y, N	f^z, N
1	0.000	0.000	$2.986\cdot 10^{-2}$	0.000	0.000	$2.975\cdot 10^{-2}$
2	0.000	$3.431\cdot 10^{-5}$	$2.943\cdot 10^{-2}$	0.000	$3.459\cdot 10^{-5}$	$2.943\cdot 10^{-2}$
3	0.000	$5.332\cdot 10^{-4}$	$1.764\cdot 10^{-2}$	0.000	$5.327\cdot 10^{-4}$	$1.766\cdot 10^{-2}$
4	0.000	0.000	$2.974\cdot 10^{-2}$	0.000	0.000	$2.975\cdot 10^{-2}$
5	$-7.700\cdot 10^{-6}$	$8.587\cdot 10^{-5}$	$2.888\cdot 10^{-2}$	$-7.487\cdot 10^{-6}$	$8.636\cdot 10^{-5}$	$2.887\cdot 10^{-2}$
6	$-7.496\cdot 10^{-6}$	$5.313\cdot 10^{-4}$	$1.834\cdot 10^{-2}$	$-7.120\cdot 10^{-6}$	$5.318\cdot 10^{-4}$	$1.833\cdot 10^{-2}$
7	0.000	0.000	$2.975\cdot 10^{-2}$	0.000	0.000	$2.975\cdot 10^{-2}$
8	$6.939\cdot 10^{-6}$	$4.858\cdot 10^{-6}$	$2.967\cdot 10^{-2}$	$6.720\cdot 10^{-6}$	$5.464\cdot 10^{-6}$	$2.968\cdot 10^{-2}$
9	$1.314\cdot 10^{-4}$	$1.352\cdot 10^{-4}$	$2.747\cdot 10^{-2}$	$1.303\cdot 10^{-4}$	$1.374\cdot 10^{-4}$	$2.745\cdot 10^{-2}$
10	0.000	0.000	$2.975\cdot 10^{-2}$	0.000	0.000	$2.975\cdot 10^{-2}$
11	$6.939\cdot 10^{-6}$	$4.858\cdot 10^{-6}$	$2.967\cdot 10^{-2}$	$6.720\cdot 10^{-6}$	$5.464\cdot 10^{-6}$	$2.968\cdot 10^{-2}$
12	$1.314\cdot 10^{-4}$	$1.352\cdot 10^{-4}$	$2.747\cdot 10^{-2}$	$1.303\cdot 10^{-4}$	$1.374\cdot 10^{-4}$	$2.745\cdot 10^{-2}$
13	0.000	0.000	$2.975\cdot 10^{-2}$	0.000	0.000	$2.975\cdot 10^{-2}$
14	$1.311\cdot 10^{-5}$	$1.321\cdot 10^{-5}$	$2.959\cdot 10^{-2}$	$1.297\cdot 10^{-5}$	$1.297\cdot 10^{-5}$	$2.959\cdot 10^{-2}$
15	$1.575\cdot 10^{-4}$	$2.259\cdot 10^{-4}$	$2.578\cdot 10^{-2}$	$1.566\cdot 10^{-4}$	$2.261\cdot 10^{-4}$	$2.578\cdot 10^{-2}$

discretised using Method no. 2 as follows: the number of ring elements was $I=300$; the number of sectors was $J=600$. In these calculations the plasma plume was bounded by a cone with vertex $2\alpha_0$ (i.e., the plasma beyond R_0 in the initial plane was conservatively neglected).

Calculation errors for the Method nos. 1 and 2 are presented in Table 3. The data from this table shows that the axial component of the force calculation error does not exceed 0.4% for all the cases. The largest component δf^x of the relative error is 5% which is obtained for the Case no. 6. At the same time the absolute error for this case is only $-3.764\cdot10^{-7}$ N. The worst case results for the other lateral force component are obtained for the Case nos. 8 and 11. The relative δf^y and absolute Δf^y errors for these cases are 12.5% and $6.060\cdot10^{-7}$ N respectively. Thus, the analysis of the calculation data allows to conclude that central projection method provides acceptable accuracy for the problem under consideration.

The calculation errors for different levels of beam discretisation, determined by the number of ring elements I, are presented in Tables 4–7. For these calculations the number of sectors in the beam is given by $I=2J$.

As can be seen from Tables 4 and 5, errors of around 10% are already achieved with $I=5$ for the cases where almost the full cone of the beam hits the target. However, the cases where a significant portion of the ion plume misses the target require a higher discretisation level. For example, for the cases in Tables 6 and 7 an error of less than 10% is reached with $I=20$.

It should also be mentioned that the functional relationship between the errors and the level of discretisation may not be monotonic, for example as it is for the Case no. 6. This feature should be taken into account to determine the minimum required level of discretisation.

7. Determination of target contour from target imaging

A digital photo camera or similar optical device can be used onboard the shepherd for the determination of the transmitted force. The objective of this device is to acquire images that allow the calculation of the central projection of the target. However, obtaining the central projection from orbital images is not a trivial task. This is due to a significant variation in the illumination conditions of the target. In order to estimate the central projection of the target from a digital image, identification of either point [18] or edge features [19,20] can be used. Edge features offer a good invariance to illumination changes or image noise and are particularly suitable for poorly textured scenes.

Taking into account that edge detection is a fundamental tool in image processing outside the scope of this paper, we will consider a simple case where the target is illuminated from the direction of the assumed thruster (Fig. 7a). This case illustrates in a simple manner how to calculate the transmitted force in orbit. At the same time the available publications about visual navigation in space using edge detection, for example [21], allow to assume that the contour of the target can be detected for the other

Table 4
Errors of calculation of transmitted forces using Method nos. 1 and 2 for Case no. 1.

I	Absolute error			Relative error		
	Δf^x, N	Δf^y, N	Δf^z, N	δf^x, %	δf^y, %	δf^z, %
3	0.000	0.000	$-8.709\cdot10^{-3}$	–	–	29.16
5	0.000	0.000	$-2.863\cdot10^{-3}$	–	–	9.59
10	0.000	0.000	$6.763\cdot10^{-4}$	–	–	2.26
20	0	0	$-6.549\cdot10^{-5}$	–	–	0.22

Table 3
Errors of calculation of transmitted forces using Method nos. 1 and 2.

No.	Absolute error			Relative error		
	Δf^x, N	Δf^y, N	Δf^z, N	δf^x, %	δf^y, %	δf^z, %
1	0.000	0.000	$1.100\cdot10^{-4}$	–	–	0.37
2	0.000	$-2.790\cdot10^{-7}$	$6.000\cdot10^{-6}$	–	0.81	0.02
3	0.000	$5.400\cdot10^{-7}$	$-1.700\cdot10^{-5}$	–	0.10	0.10
4	0.000	0.000	$-7.000\cdot10^{-6}$	–	–	0.02
5	$-2.125\cdot10^{-7}$	$-4.950\cdot10^{-7}$	$9.000\cdot10^{-6}$	2.76	0.57	0.03
6	$-3.764\cdot10^{-7}$	$-4.20\cdot10^{-7}$	$1.500\cdot10^{-5}$	5.02	0.08	0.08
7	0.000	0.000	$-3.000\cdot10^{-6}$	–	–	0.01
8	$2.189\cdot10^{-7}$	$-6.060\cdot10^{-7}$	$-4.000\cdot10^{-6}$	3.15	12.47	0.01
9	$1.110\cdot10^{-6}$	$-2.260\cdot10^{-6}$	$1.800\cdot10^{-5}$	0.84	1.67	0.06
10	0.000	0.000	$-3.000\cdot10^{-6}$	–	–	0.01
11	$2.189\cdot10^{-7}$	$-6.060\cdot10^{-7}$	$-4.000\cdot10^{-6}$	3.15	12.47	0.01
12	$1.110\cdot10^{-6}$	$-2.260\cdot10^{-6}$	$1.800\cdot10^{-5}$	0.84	1.67	0.06
13	0.000	0.000	$-5.000\cdot10^{-6}$	–	–	0.01
14	$1.360\cdot10^{-7}$	$2.370\cdot10^{-7}$	$-1.000\cdot10^{-6}$	1.04	1.79	0.01
15	$9.500\cdot10^{-7}$	$-1.900\cdot10^{-7}$	$5.000\cdot10^{-6}$	0.60	0.08	0.02

cases of the target illumination using more sophisticated image processing algorithms.

When using photos of the target for the definition of the transmitted force with the above approach, it is necessary to determine the coordinates of the points of the contour of its image on a projection plane in F_P. The following additional frames of reference are defined for this purpose.

The frame $O_S x_S y_S z_S$ is connected to the sensitive element of the camera (F_S), whose origin O_S is fixed in the optical centre of the plane of projection. The axis $O_S z_S$ is perpendicular to the plane of projection and is directed toward the target; axes $O_S x_S$ and $O_S y_S$ are parallel to the central axes of symmetry of the sensitive element. We will consider that the camera is mounted in such a way that the corresponding axes of frames $O_S x_S y_S z_S$ and $O_P x_P y_P z_P$ are parallel.

Table 5
Errors of calculation of transmitted forces using Method nos. 1 and 2 for Case no. 3.

I	Absolute error			Relative error		
	Δf^x, N	Δf^y, N	Δf^z, N	δf^x, %	δf^y, %	δf^z, %
3	0.000	$1.560 \cdot 10^{-4}$	$7.970 \cdot 10^{-3}$	–	29.26	45.19
5	0.000	$-1.001 \cdot 10^{-5}$	$2.712 \cdot 10^{-3}$	–	1.88	15.37
10	0.000	$3.010 \cdot 10^{-5}$	$2.499 \cdot 10^{-3}$	–	5.64	14.17
20	0.000	$-1.038 \cdot 10^{-5}$	$1.145 \cdot 10^{-3}$	–	1.95	6.49
50	0.000	$4.316 \cdot 10^{-6}$	$5.298 \cdot 10^{-4}$	–	0.81	3.00
100	0.000	$-1.792 \cdot 10^{-6}$	$2.394 \cdot 10^{-4}$	–	0.34	1.35
200	0.000	$9.178 \cdot 10^{-7}$	$1.542 \cdot 10^{-4}$	–	0.17	0.87

Table 6
Errors of calculation of transmitted forces using Method nos. 1 and 2 for Case no. 4.

I	Absolute error			Relative error		
	Δf^x, N	Δf^y, N	Δf^z, N	δf^x, %	δf^y, %	δf^z, %
3	0.000	0.000	$-8.826 \cdot 10^{-3}$	–	–	29.67
5	0.000	0.000	$-2.980 \cdot 10^{-3}$	–	–	10.02
10	0.000	0.000	$5.593 \cdot 10^{-4}$	–	–	1.88
20	0.000	0.000	$-1.825 \cdot 10^{-4}$	–	–	0.61

The origin O_C of the reference frame connected with the camera (F_C) $O_C x_C y_C z_C$ is arranged on the focal point of the camera. The axes of F_S and F_C coincide.

Let us obtain the grey scale image of a target (Fig. 7a). We will consider that the camera matrix has N pixels along the abscissa axis and M along the ordinate axis. Then such an image can be described by a matrix G. Each element of this matrix g_{nm} ($n = 1, \ldots, N$; $m = 1, \ldots, M$) can have a value in the range from 0 to s, where s is the number of levels of gray. Choosing some threshold value for g_{nm}, we will transform the image G into binary (Fig. 7b) which we will designate as the matrix B. Elements b_{nm} of this matrix are 0 or 1, depending whether g_{nm} is lower or higher than the threshold value. The following step of handling the image is to identify the pixels from the matrix B which are located on the black and white boundary and form the target contour (Fig. 7c). This contour is represented by the matrix C which has dimensions $K \times 2$, where K is the number of the points forming the contour. Elements of this matrix c_{k1} and c_{k2} are horizontal and vertical pixel indices (k-point) of the contour. Thus, the contour points are set by the indices of corresponding pixels. Using matrix elements C one can obtain the coordinates of the contour points in F_S as follows

$$x_S^k = \Delta(c_{k1} - n/2),\ y_S^k = \Delta(c_{k2} - m/2), \tag{15}$$

where Δ is the size of the pixel of the camera matrix.

When the camera is installed in such a manner that its focal point coincides with the vertex of the cone of the beam, and its focal length is equal to f, frames F_S and F_P coincide and expressions (12) define the coordinates of the required contour. Here it is necessary to notice that, while choosing the projection plane at a distance equal to the camera focal length is not hard, installing the camera at the vertex of the beam cone is problematic from an engineering point of view. Therefore, we will consider the case where the camera is positioned with a small shift or offset (0.1 … 0.2 m) relative to the beam axis. Such a shift will cause the contour of the target obtained from the photos to differ from the contour that should be used in the proposed algorithm. This phenomenon is visible in Fig. 8 for the target considered in Section 6. Line 1 represents the contour corresponding to the case where the focal point of the camera coincides with the vertex of the cone of the beam, and line 2 shows a contour for the case where the camera is offset by 0.2 m along the axis of ordinates.

Table 7
Errors of calculation of transmitted forces using Method nos. 1 and 2 for Case no. 6.

I	Absolute error			Relative error		
	Δf^x, N	Δf^y, N	Δf^z, N	δf^x, %	δf^y, %	δf^z, %
3	$-7.496 \cdot 10^{-6}$	$-1.659 \cdot 10^{-4}$	$-9.443 \cdot 10^{-4}$	100.00	31.22	5.19
5	$-3.493 \cdot 10^{-6}$	$-7.309 \cdot 10^{-4}$	$1.616 \cdot 10^{-3}$	46.59	13.75	8.81
10	$-5.388 \cdot 10^{-6}$	$1.573 \cdot 10^{-5}$	$2.506 \cdot 10^{-3}$	71.87	2.96	13.66
20	$2.599 \cdot 10^{-6}$	$-1.458 \cdot 10^{-5}$	$9.290 \cdot 10^{-4}$	34.66	2.74	5.06
50	$4.084 \cdot 10^{-7}$	$1.452 \cdot 10^{-6}$	$5.179 \cdot 10^{-4}$	5.45	0.27	2.82
100	$1.676 \cdot 10^{-7}$	$-3.245 \cdot 10^{-6}$	$2.152 \cdot 10^{-4}$	2.23	0.61	1.17
200	$1.089 \cdot 10^{-7}$	$1.286 \cdot 10^{-7}$	$1.372 \cdot 10^{-4}$	1.45	0.02	0.79

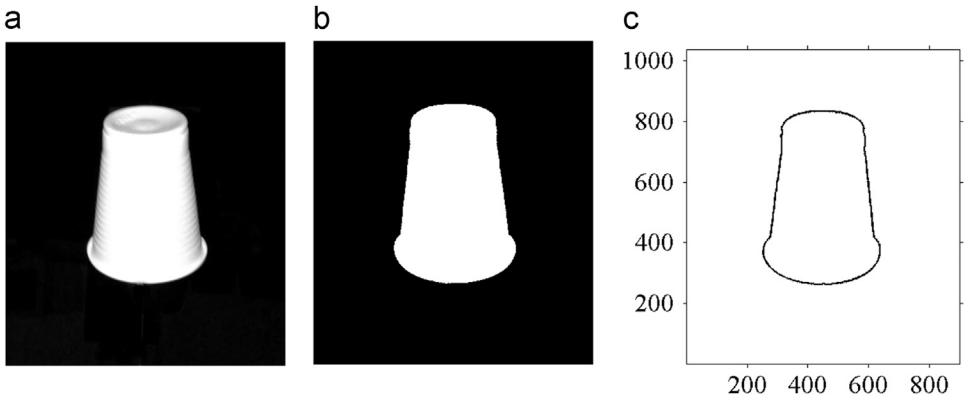

Fig. 7. Digital image processing of an example target.

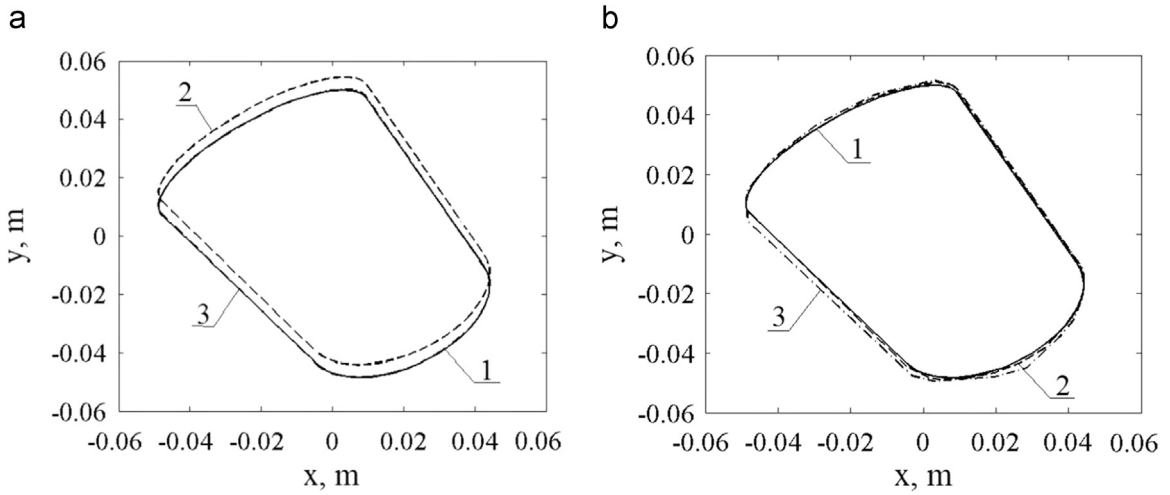

Fig. 8. Contours of target projection.

Let us consider a possible correction of the coordinates of the contour obtained with use of the expressions (15) to account for this offset. The vectors defining the set of target points in F_C can be found as follows:

$$\mathbf{P}_C^l = \mathbf{P}_T^l + \mathbf{L}_{TC}, \tag{16}$$

where $\mathbf{L}_{TC} = \begin{bmatrix} \tilde{x} & \tilde{y} & \tilde{z} \end{bmatrix}^T$ is the vector defining the position of the F_C origin in F_G.

Taking into account expressions (8) and (15), the coordinates of the target points projected on the plane of the camera matrix may be defined as follows:

$$x_S^l = f\frac{x_T^l + \tilde{x}}{z_T^l + \tilde{z}},\ y_S^l = f\frac{y_T^l + \tilde{y}}{z_T^l + \tilde{z}}. \tag{17}$$

Since it is possible to choose a location for the camera for which $\tilde{z} = 0$, comparing formulas (8) and (14) it is possible to write the expressions for the coordinates of the contour taking into account the camera offset:

$$x_P^l = x_S^l - \frac{\tilde{x}}{z_T^l},\ y_P^l = y_S^l - \frac{\tilde{y}}{z_T^l}. \tag{18}$$

However, expressions (18) cannot be used directly to correct the contour since it is obviously not possible to define the magnitude of z_T^l for each considered point. Nevertheless, instead of the exact values for z_T^l it is possible to use an approximate value. For example, for all points it is possible to use z_0 that is the distance from the vertex of the cone of the beam to the geometric centre of the target. Taking this into account, expression (18) gives

$$x_P^l \approx x_P^l - \frac{\tilde{x}}{z_0},\ y_P^l \approx y_S^l - \frac{\tilde{y}}{z_0}. \tag{19}$$

In Fig. 8a, line 3 represents corrected contour calculated with use of expression (18) and using the photo that is obtained by the shifted camera. In this figure it is apparent that the corrected contour practically coincides with the contour obtained by a camera without offset (line 1).

In Fig. 8b the corrected contour of the target when there is an inaccuracy in the determination of the position of its geometric centre is presented. When carrying out the calculations, it is accepted that the error in the determination of the geometric centre represents a random variable with a normal distribution law and zero expectation. The contours 2 and 3 are obtained for the mean squared deviation of the error respectively $\sigma = 1$ m and $\sigma = 1.5$ m.

As can be seen in Fig. 8b, satisfactory results are obtained even for a rough determination of the relative position of the centre of mass. The necessary accuracy in

the definition of the position of the geometric centre can be ensured by using existing hardware, for example on the basis of remote sensing technology that measures distance by illuminating the target with a laser and analysing the reflected light (LIDAR).

8. Algorithm for the calculation of the transmitted force

The general algorithm for the calculation of the transmitted force can be summarised into the following steps.

1 Choice of the plane of projection.
2 Partition of the central projection of the GIT beam into finite elements.
3 Definition of the contour of the central projection of the target.
  3.1. To solve the modelling problems:
    3.1.1. Approximation of the surface of the target by a mesh of finite elements.
    3.1.2. Projection of the points of the mesh on the chosen plane with use of the expressions (8).
    3.1.3. Calculation of the contour of the target projection by constructing the convex or non-convex hull of the target.
  3.2. After photos are obtained in orbit:
    3.2.1. Transformation of the initial image into a binary matrix.
    3.2.2. Definition of the pixels that form the contour of the target projection.
    3.2.3 Calculation of the coordinates of the polygon vertices that approximate the contour of the target, with the use of (15).
    3.2.4. Correction of the errors due to the camera offset with expressions (18).
4 Identification of the finite beam elements hitting the area bounded by the contour of the target projection using the solution of the problem of belonging of a point to a polygon.
5 Calculation of the elementary force vectors at the finite elements selected on the previous step with the use of the formulas (10)–(13).
6 Calculation of the vector of the transmitted force by summation of the elementary forces (14).

9. Conclusions

The problem of the determination of the force transmitted by an ion beam to a downstream target in the context of contactless space debris removal has been addressed in this paper. The method and algorithms proposed here possess essential advantages in comparison to those that use direct integration of the transmitted forces over the object surface, regarding the need of information about the exact shape, size and attitude of the space debris object. In the proposed algorithm, only information on the contour of its central projection on a plane is required. To obtain the image of the target central projection in orbit it is proposed to use an optical camera. Algorithms for the determination of the target contour and identification of the plasma beam elements hitting the target have been developed. Problems of inaccuracy in the determination of the target contour due to a mismatch of the focal point of the camera with the vertex of the ion beam envelop cone have been investigated, and algorithms for the correction of this inaccuracy have been proposed. Numerical calculations to validate the method have been carried out. The general algorithm to process the photos and determine the target contour has been presented. An additional study in this area taking into account real images obtained in orbit should be carried out to ensure a robust target contour detection.

Acknowledgements

The research leading to these results has received funding from the European Union Seventh Framework Programme (FP7/2007-2013) under grant agreement No. 607457.

References

[1] J.-C. Liou, A.K. Anilkumar, B. Bastida, et al., Stability of the Future Leo Environment – an IADC Comparison Study, In: Proceedings of the 6th European Conference on Space Debris, (ESA SP-723, August 2013), Darmstadt, Germany, April, 2013, pp. 22–25.
[2] S. Bondarenko, S. Lyagushin, G. Shifrin, Prospects of using lasers and military space techlogy for space debris removal, In: Proceedings of the 2nd European Conference on Space Debris, 1997.
[3] C.R. Phipps, J.P. Reilly, ORION: clearing near-Earth space debris in two years using a 30-kW repetitively-pulsed laser, In: SPIE Proc. Int. Soc. Opt. Eng. 1997.
[4] C. Bombardelli, J. Herrera, A. Iturri, J. Pelaez, Space debris removal with bare electrodynamic tethers, In: Proceedings of the 20th AAS/AIAA Spaceflight Mechanics Meeting, San Diego, CA., 2010.
[5] N. Takeichi, Practical operation strategy for deorbit of an electrodynamic tethered system, J. Spacecr. Rocket. 43 (6) (2006) 1283–1288, http://dx.doi.org/10.2514/1.19635.
[6] J. Sanmartin, et al., An universal system to de-orbit satellites at end of life, J. Space Technol. Sci. 26 (1) (2012) 21–32.
[7] C. Bombardelli, D. Zanutto, E. Lorenzini, Deorbiting performance of bare electrodynamic tethers in inclined orbits, J. Guid. Control. Dyn. 36 (5) (2013) 1550–1556.
[8] G. Sánchez-Arriaga, C. Bombardelli, X. Chen, Impact of nonideal effects on bare electrodynamic tether performance, J. Propuls. Power 31 (3) (2015) 951–955.
[9] C. Bombardelli, J. Peláez, Ion beam shepherd for contactless space debris removal, J. Guid. Control. Dyn. 34 (3) (2011) 916–920.
[10] T. Trottenberg, J. Rutcher, H. Kersten, Experimental investigation of momentum transfer to solid surfaces by the impact of energetic ions and atoms, In: Proceedings of the 33rd International Electric Propulsion Conference, paper IEPC-2013-329, Washington, 2013.
[11] F. Cichocki, M. Merino, E. Ahedo, Modeling and simulation of EP plasma plume expansion into vacuum, In: Proceedings of the 50th AIAA/ASME/SAE/ASEE Joint Propulsion Conference, 2014.
[12] M. Merino, F. Cichocki, E. Ahedo, Collisionless plasma thruster plume expansion model, Plasma Sources Sci. Technol., 2015. (currently under review).
[13] C. Bombardelli, M. Merino, E. Ahedo, J. Peláez, H. Urrutxua, A. Iturri-Torreay, J. Herrera-Montojoy, Ariadna call for ideas: active removal of space debris ion beam shepherd for contactless debris removal, Technical report, 2011.
[14] C. Bombardelli, H. Urrutxua, M. Merino, E. Ahedo, J. Peláez, Relative dynamics and control of an ion beam shepherd satellite, Spacefl. Mech. 143 (2012) 2145–2158.
[15] P.J. Frey, P.L. George, Mesh Generation Application to Finite Elements, HERMES Science Europe Ltd. Paris, France, 2000.

[16] M. De Berg, M. Van Kreveld, M. Overmars, O. Schwarzkopf, Computational Geometry: Algorithms and Applications, Springer, NY, 2000.
[17] M. Duckham, L. Kulik, M. Worboys, A. Galton, Efficient generation of simple polygons for characterizing the shape of a set of points in the plane, Pattern Recognit. 41 (10) (2008) 2965–3270.
[18] (a) K. Hormann, A. Agathos, The point in polygon problem for arbitrary polygons, Comput. Geom. Theory Appl. 20 (2001) 131–144;
(b) G. Bleser, Y. Pastarmov, D. Stricker, Real-time 3d camera tracking for industrial augmented reality applications, in: WSCG 2005 Conference Proceedings, January 31–February 4, 2005, Plzen, Czech Republic, UNION Agency, Science Press, ISBN 80-903100-7-9.
[19] D.G. Lowe, Fitting parameterized threedimensional models to images, IEEE Trans. Pattern Anal. Mach. Intell. 13 (5) (1991) 441–450.
[20] T. Drummond, R. Cipolla, Real-time visual tracking of complex structures, IEEE Trans. Pattern Anal. Mach. Intell. 24 (7) (2002) 932–946.
[21] K. Kanani, A. Petit, E. Marchand, T. Chabot, B. Gerber, Vision based navigation for debris removal missions, In: Proceedings of 63rd International Astronautical Congress 2012, 1–5 October, Naples, Italy, 2012, IAC-12-A6-5-9-x14900.